Experimental Study on the Confinement of Concrete Cylinders with Large Rupture Strain FRP Composites

Nicholas Sirach[1]; Scott T. Smith[2*], F.ASCE; Tao Yu[3], M.ASCE; Ahmed Mostafa[4]

1. PhD candidate, Faculty of Science and Engineering, Southern Cross University, Lismore, NSW, 2480, Australia, E: n.sirach.10@student.scu.edu.au

2. Professor, School of Civil, Environmental and Mining Engineering, The University of Adelaide
Adelaide, SA, 5005, Australia, E: scott.smith@adelaide.edu.au (* Corresponding Author)

3. Professor, Department of Civil and Environmental Engineering, The Hong Kong Polytechnic University, Hong Kong, China, E: tao-cee.yu@polyu.edu.hk

4. Senior Lecturer, Faculty of Science and Engineering, Southern Cross University, Lismore, NSW, 2480, Australia, E: ahmed.thabet@scu.edu.au

Abstract

Large rupture strain (LRS) fibre-reinforced polymer (FRP) composites, typically formed from polyethylene naphthalate (PEN) and polyethylene terephthalate (PET) fibres, generally exhibit ultimate rupture strains greater than 5 %. Such fibres are particularly suited to the confinement of concrete columns on account of their large rupture strains and sufficient elastic modulus. There are currently a limited number of studies on LRS FRP-confined concrete, particularly with high- and ultra-high-strength concrete, so their behaviour across a range of variables is still unknown. To improve this understanding, this paper systematically investigates the influence fibre type, fibre thickness and concrete strength have on the behaviour of FRP-confined concrete. To achieve this objective, the current investigation presents the results of 66 circular FRP-confined cylinders that are loaded concentrically. Three main parameters are investigated, namely, fibre type (i.e. PEN, PET, carbon, glass, aramid), concrete strength (i.e. normal-, high- and ultra-high-strength), and fibre thickness. The results show that regardless of

fibre type, the stress-strain response is bilinear when the concrete is sufficiently confined. However, when there is insufficient confinement provided to the concrete core, the stress-strain response becomes trilinear. This trilinear response is more pronounced for LRS FRP-confined specimens since the confinement stiffness of the LRS FRP jacket is lower than a traditional FRP-confined specimen with an equivalent confinement ratio. Increasing the confining hoop stiffness (i.e. increasing FRP layers) reduces the magnitude of strength reduction after initial concrete cracking. It is also evident that as the unconfined concrete strength increases, the minimum confinement stiffness ratio necessary to prevent strength reduction after initial concrete cracking increases.

Author Keywords

FRP; Large rupture strain; LRS; PET; PEN; concrete; confinement; ultra-high-strength

Introduction

A common utilisation of fibre-reinforced polymer (FRP) composites in the building industry is the wrapping of existing reinforced concrete (RC) columns for strengthening and retrofitting purposes (Teng et al. 2002; Ozbakkaloglu and Akin 2012; Isleem et al. 2018; Zeng et al. 2018). To facilitate this application, FRP jackets are used to wrap existing RC columns to provide lateral confinement, thus improving the strength and ductility capacity of the column. Several models that could be used in design and analysis have been developed to capture an accurate representation of the axial stress-strain behaviour of these columns under concentric compression (e.g. Lam and Teng 2003; Jiang and Teng 2007; Teng et al. 2009). Most of these models have been developed and validated using FRP composites that typically exhibit ultimate

rupture strains of less than 3 %. These FRP composites are aramid FRP (AFRP), glass FRP (GFRP), and carbon FRP (CFRP), and are herein referred to as *traditional FRPs*.

The tensile stress-strain response of traditional FRPs is linear elastic and the failure mode is brittle rupture. Failure of a confined concrete column typically occurs when the FRP jacket ruptures as a result of lateral expansion of the concrete core, which occurs at a lower tensile strain than that obtained from FRP coupon tensile tests (Xiao and Wu 2003; Smith et al. 2010; Ozbakkaloglu et al. 2013). Given this relationship, concrete that is confined by an FRP composite with a low ultimate rupture strain exhibits less dilation than concrete that is confined by a large rupture strain (LRS) FRP composite. Specifically for the function of seismic retrofitting, where enhancing the axial deformation is critical, the use of an FRP jacket containing LRS fibres can be greatly beneficial as the same level of strength enhancement can be achieved with far greater deformation capacity in comparison to using a traditional FRP jacket with a lower rupture strain (Dai et al. 2011; Saleem et al. 2018).

In light of the above, a number of FRP composites have emerged as viable alternatives to traditional FRPs for seismic retrofit confinement applications (Anggawidjaja et al. 2006; Dai et al. 2011; Bai et al. 2014; Zhang et al. 2017a; Ispir et al. 2018). These FRP composites, namely polyethylene terephthalate (PET) and polyethylene naphthalate (PEN), possess a bilinear tensile stress-strain response with a large rupture strain and low elastic modulus. LRS FRP composites are environmentally beneficial and relatively economical when compared to traditional FRP composites since they are manufactured from recycled plastic materials such as water bottles.

Given the increasing desire for use of recycled materials in construction, these LRS FRP composites offer a highly attractive alternative to traditional FRP composites.

High-strength concrete (HSC) has become a commonly used construction material in recent years, particularly in multi-storey buildings, due to the superior performance and economic benefits it provides over normal-strength concrete (NSC). Based on existing studies and for the context of this paper, NSC has a compressive strength of less than 50 MPa, HSC has a compressive strength in the range of 50 – 100 MPa, and ultra-high-strength concrete (UHSC) has a compressive strength in excess of 100 MPa (Xiao et al. 2010; Vincent and Ozbakkaloglu 2013; Zeng et al. 2020). A shortcoming of higher strength concrete is that as the strength of the concrete increases, it becomes stiffer and has less deformation capacity. Studies have shown that when HSC is incorporated in hybrid structures (i.e. concrete and FRP), it is highly attractive since the efficient combination of high performance materials can result in high axial strength and large deformation capacity (Xie and Ozbakkaloglu 2015; Zhang et al. 2017b; Wang et al. 2019). For this reason, it is anticipated that the use of LRS FRP with HSC is attractive due to the potential of developing a structure that not only has very high strength, but is extremely ductile. While several researchers have assessed the behaviour of LRS FRP-confined NSC (Dai et al. 2011; Bai et al. 2014; Ispir 2015; Saleem et al. 2017; Ispir et al. 2018; Han et al. 2020) and traditional FRP-confined HSC and UHSC (Ozbakkaloglu 2013a; Vincent and Ozbakkaloglu 2013; Zhang et al. 2020), only one study to date has evaluated the performance of LRS FRP-confined HSC and UHSC (Zeng et al. 2020).

For LRS FRP composites to be utilised in industry, accurate stress-strain models must be developed to enable design and analysis of such column systems. The majority of stress-strain models for FRP-confined concrete have been developed and validated using data obtained from traditional FRP-confined column tests. Recent studies have shown that direct application of these existing stress-strain models for LRS FRP-confined concrete columns could lead to unconservative design (Dai et al. 2011; Ispir 2015; Bai et al. 2019). A few studies in recent years have modified and improved existing stress-strain models for FRP-confined concrete with LRS FRP experimental results to enable better predictions of the stress-strain behaviour of LRS FRP-confined concrete (Dai et al. 2011; Bai et al. 2019; Zeng et al. 2020).

For such stress-strain models to be adopted in design, they must be capable of accurately capturing the stress-strain response of LRS FRP-confined concrete columns over a range of test variables. With a limited number of experimental studies on the compressive behaviour of LRS FRP-confined concrete, the accuracy of these models over a wide range of test parameters are still unknown. These models have been developed and verified using a limited number of test specimens due to the scarce data available in the literature. Furthermore, only Zeng et al. (2020) accounted for the strength reduction after initial concrete cracking of LRS FRP-confined HSC and UHSC in their model, and this model was only developed and verified for HSC and UHSC confined with PET FRP test specimens that were published in their study. There is a need for additional experimental test data on LRS FRP-confined concrete, particularly for LRS FRP-confined HSC and UHSC.

Prior to undertaking the testing contained herein, no known studies existed on the compressive behaviour of LRS FRP-confined HSC and UHSC. Since then, Zeng et al. (2020) published a study on the monotonic behaviour of PET FRP-confined HSC and UHSC. While Zeng et al. (2020)'s work tested a number of similar specimens to this study, there are some noticeable differences. In Zeng et al. (2020)'s study, prefabricated PET FRP tubes were used to confine concrete ranging from NSC to UHSC. A trilinear stress-strain response was observed for PET FRP-confined specimens across all concrete strengths, including NSC. From this study, it is inconclusive if shrinkage is playing a major role in the trilinear response since prefabricated PET FRP tubes were used, or if it is an inherent mechanism within LRS FRP confinement of high strength concrete. In addition, Zeng et al. (2020) focused on the use of PET FRP and did not investigate the behaviour of the other commonly used LRS fibre, PEN FRP, or any traditional FRP composites.

With the limited number of experimental studies on LRS FRP-confined concrete, particularly those containing high and ultra-high strength concrete, the accuracy and reliability of recently developed stress-strain models for LRS FRP-confined concrete columns over a range of different test parameters are still unknown. This paper aims to expand the knowledge and test database of concrete columns confined with LRS FRP through an experimental study that includes NSC, HSC and UHSC confined with both traditional and LRS FRP composites. Although solely experimental, the results are presented in sufficient detail for use by researchers in the future to develop and validate new and existing constitutive models for both traditional and LRS FRP-confined concrete over a range of different concrete strengths. Commentary on

the stress-strain behaviour of LRS FRP-confined concrete is provided to give insights on the confinement mechanism of LRS FRP-confined concrete, particularly for the trilinear stress-strain response of LRS FRP-confined HSC and UHSC. To date, only PET FRP has been tested with HSC and UHSC, so it is still unclear how a stronger, less ductile bilinear FRP material (i.e. PEN FRP) behaves when confining HSC and UHSC. To bridge this gap, this paper presents the first experimental results on PEN FRP-confined HSC and UHSC. In essence, this paper systematically investigates the influence of fibre type, fibre thickness and concrete strength on the behaviour of FRP-confined concrete.

Experimental Programme

Test Programme

A total of 66 FRP-confined concrete cylinders of nominal 150 mm diameter and 300 mm height, which were subjected to concentric axial compression, were tested to failure under the application of monotonic loading. The parameters investigated in this study were concrete strength, fibre type and fibre thickness. Three different concrete strengths were designed and cast for this study and they fall within the ranges of NSC, HSC and UHSC. The specimens were confined with FRP arising from five different fibre types, namely PEN FRP, PET FRP, AFRP, CFRP, and GFRP, with varying thicknesses of one to four fibre sheet layers.

The details of the test specimens are provided in Tables 1 to 3. The labelling convention adopted is based on fibre type (A = aramid, C = carbon, G = glass, PEN = polyethylene naphthalate, PET = polyethylene terephthalate), concrete strength (NS = normal-strength, HS = high-strength, UHS = ultra-high-strength), number of fibre sheet layers (e.g. 1 = one layer, 2 = two

layers), and a letter to identify two nominally identical specimens (a or b). For example, PET-HS-2-b refers to the second specimen of two nominally identical FRP-confined high strength concrete specimens containing two layers of PET FRP.

When designing the test programme, careful consideration was given to the number of fibre sheet layers applied to each specimen. It is well documented that the confinement pressure heavily influences the behaviour of FRP-confined concrete, thus this value was kept as consistent as possible for specimens confined with different fibre types. The nominal confinement ratio (f_l/f'_{co}) is used to establish relative confinement levels across specimens with varying FRP jackets and different concrete strengths. It is expressed as $f_l/f'_{co} = 2E_f t_f \varepsilon_f / Df'_{co}$. This approach of using the nominal confinement ratio is consistent with existing studies that compare FRP type (Ozbakkaloglu 2013b; Ozbakkaloglu and Xie 2016).

Since the tensile stress-strain response of PEN and PET FRP is bilinear in nature, there are distinct first and second elastic modulus values (E_1 and E_2, respectively) in the responses. Figure 1 shows the tensile stress-strain response of these LRS FRP composites. When calculating the nominal confinement ratio for PEN and PET FRP-confined specimens, the elastic modulus (E_f) and the strain capacity of the fibres (ε_f) is replaced with the ultimate tensile stress of the fibres (f_f) since the response is bilinear. Therefore, it is expressed as $f_l/f'_{co} = 2f_f t_f / Df'_{co}$.

FRP Composites

Flat coupon tests were undertaken on five samples for each FRP composite in accordance with ASTM D 7565 (2017) and the results are provided in Table 4. Five fibre types were tested in

this study, namely AFRP, CFRP, GFRP, PEN FRP, and PET FRP. A two-part epoxy resin was used for each FRP type, namely Sicomin SR 8100 resin and Sicomin SD 8824 hardener, and the properties for this material can be found in Table 4. The FRP coupons had a width of 20 mm and a length of 250 mm. Two uniaxial strain gauges were positioned at the mid-height of each specimen (one each side) to measure the axial deformation of the FRP. These 10 mm strain gauges had a gauge factor of 2.10 ± 1 % and a gauge resistance of 118.5 ± 0.5 Ω. In addition, aluminium tabs of 20 mm width and 50 mm length were bonded onto the ends of the cured FRP coupons prior to testing to prevent crushing of the test coupon by the test machine grips. For each FRP composite, the average tensile strength and ultimate tensile strain in the longitudinal direction are provided in Table 4. For the CFRP, GFRP and AFRP composites, the average elastic modulus is also provided. Due to the bilinear nature of PET and PEN FRP, the first and second elastic modulus values are provided (E_1 and E_2). In addition, the constant strength value ($C_{f,0}$) where the extrapolation of the second linear branch intersects the vertical axis (σ_f) is provided for PEN and PET FRP, as well as the strain at which the two linear branches intersect ($\varepsilon_{f,0}$). The stress-strain responses of the PEN and PET FRP coupons are shown in Figure 1.

Concrete

Three separate batches of concrete were cast for this study in accordance with AS1012.2 (2014). For each concrete batch, five plain cylinders were cast and tested to evaluate the compressive properties of the unconfined concrete. These properties were tested and determined in accordance with AS1012.9 (2014) at the same time the FRP-confined cylinders were tested. The first batch of concrete (herein referred to as *NSC*) had an unconfined concrete strength and corresponding compressive strain of 20.9 MPa and 0.0019, respectively. The second batch of

concrete (herein referred to as *HSC*) had respective values of 52.7 MPa and 0.0021, respectively. The third batch of concrete (herein referred to as *UHSC*) had respective values of 110.9 MPa and 0.0026.

Sample Preparation

All concrete cylinders were left to cure in a laboratory at room temperature for at least 30 days prior to FRP wrapping to minimise any possible concrete shrinkage after wrapping. Prior to wrapping, the top surface of the concrete samples were lightly grinded (~1-2 mm) to remove any mortar rich areas and to ensure the top and bottom surfaces were parallel to each other and perpendicular to the sides. The FRP composites were applied to the surface of the concrete using the wet lap-up method (Teng et al. 2002). Prior to wrapping, the fibres were impregnated, and the concrete surface was brushed with epoxy. Irrespective of the number of fibre sheet layers used for each sample, a continuous unidirectional fibre sheet, with the unidirectional fibres oriented in the circumferential (hoop) direction, was used to wrap the samples. Each sample had an overlapping zone of at least 150 mm, which is approximately one third of the circumference of each concrete cylinder. Because of the thickness of the PEN and PET FRP, additional length of material was used to achieve an overlapping length of 150 mm. Regardless of the FRP type, each specimen had its ends strengthened with 25 mm wide CFRP strips to prevent premature FRP failure at these locations. Once wrapped, these samples were cured in laboratory conditions with a temperature ranging between 20 - 22 °C and humidity ranging between 70 – 75 % for at least seven days. After the FRP wraps had undergone full curing, any excess FRP material from the ends of the sample was carefully removed by grinding.

Test Set-up and Instrumentation

The axial deformation of each FRP-confined specimen was recorded using two pairs of linear variable displacement transducers (LVDTs), as shown in Figure 2(a). Both pairs of LVDTs were placed on the same diametrically opposite sides of the specimen. One pair was fastened to the specimen using plastic ties and was used to measure the mid-height deformation of the specimen over a 150 mm gauge length. The other pair was attached to the test machine and was used to measure the overall movement between the testing platens.

Five unidirectional strain gauges were bonded onto each specimen outside the overlapping region of the FRP jacket as indicated schematically in Figure 2(b). Two strain gauges were used to measure axial deformations and three strain gauges were used to measure lateral deformations. All five strain gauges were bonded onto the specimens at mid-height. These strain gauges had a gauge length of 20 mm, a gauge factor of 2.12 ± 1 %, and a gauge resistance of 120 ± 0.5 Ω.

All specimens were tested under monotonic axial compression using a 10 MN compression testing machine. The tests were operated under a displacement-controlled mode at a constant rate of 0.6 mm/min. To ensure uniform loading, high-strength gypsum was used to cap the top and bottom surfaces of the specimens prior to testing. Additionally, two thick mild steel plates were used to transfer load from the test machine platens to the cylinder. All samples were initially loaded to approximately one-fifth of their unconfined concrete strength in order to confirm vertical alignment (i.e. concentric load), followed by near load removal and then testing.

A data logging system simultaneously recorded all the test data, including loads, displacements and strains.

Test Results and Discussions

Failure Modes

The failure of LRS FRP-confined concrete always occurred outside the overlapping zone and was typically confined to a small vertical portion in the mid-height of the sample (Figure 3(a-b)). Similar failures were noted for the traditional FRP-confined specimens, however the fibres ruptured over a larger vertical span (Figure 3(c-e)). It is expected that the pronounced effect of bulging at the mid-height region of the column due to excessive concrete dilation is the cause of FRP rupture localisation at the mid-height of LRS FRP-confined specimens. It is evident in Figure 4 that the failure mechanism of the internal concrete core changed as the concrete strength increased. As seen in Figure 4(a), no large cracks are evident and there are only small uniform crack formations in the NSC at failure. Similarly in Figure 4(b), the HSC also has small uniform crack formations, with larger cracks also present. Figure 4(c) shows the failure of UHSC, and it is apparent that the failure of the concrete has changed from small uniform cracks to larger, localised cracks. An observation made after testing was that the FRP rupture in the UHSC specimens was often initiated at the location of these large localised cracks. Apart from this, the concrete strength appeared to have little influence on the failure mode of both traditional FRP- and LRS FRP-confined specimens.

There were several LRS FRP-confined specimens that failed due to slippage between the FRP layers (refer to Tables 1-2). Typical FRP slippage failures are shown in Figure 5. Similar failures

were noted by other researchers for LRS FRP-confined concrete (Dai et al. 2011; Ispir 2015; Saleem et al. 2017; Zeng et al. 2020). These studies predominately attributed the slippage failures to insufficient overlapping of the FRP or unsuitable epoxy. It was noted in these studies that although the overlapping length was calculated based on the circumference of the specimen, the overlapping length was fixed for all specimens tested. This was also the case for the specimens tested in this study, with a fixed overlapping length of 150 mm being used for all specimens. Due to the thickness of the PEN and PET FRP, increasing the number of FRP layers will result in a considerable increase in the outside circumference of the specimens. Since the overlapping length was calculated based on the circumference of the concrete core, the change in external circumference is no longer negligible once the FRP jacket is sufficiently thick. This increases the one-third of the circumference requirement from 150 mm to approximately 180 mm for three- and four-layer LRS FRP. It is feasible that this is one of the reasons that slippage occurred between FRP layers in not only this study, but existing studies too. As a result, it is recommended to use an overlapping length of half the outside circumference of the LRS FRP jacket to avoid premature slippage failures, particularly for jackets with one or two layers. Additionally, it was observed during testing that lateral dilation of the mid-height region was excessive for LRS FRP-confined samples, particularly those confined with PET FRP. This excessive dilation can induce both tensile and bending stresses onto the unidirectional fibre sheet and hence assist in premature debonding of the FRP in the overlapping region. It is expected that the premature failure of the LRS FRP can be attributed to a combination of the causes mentioned above.

Axial Stress-Strain Response

The typical compressive stress-axial strain response for the specimens tested in this study can be separated into two main categories, namely (i) those specimens that exhibit two distinct branches connected by a transition zone (Figure 6(a)), and (ii) those samples that exhibit a post-peak strength reduction after initial concrete cracking and before full FRP activation (Figure 6(b)). For the purpose of discussion, the former will be referred to as a bilinear response (Lam and Teng 2003) and the latter as a trilinear response (Saleem et al. 2017).

For both the bilinear and trilinear response of FRP-confined concrete shown in Figure 6, the first branch is that of an ascending curve that reflects the behaviour of unconfined concrete. For the bilinear response of FRP-confined concrete shown in Figure 6(a), this initial branch is followed by a curved transition zone where the concrete is cracking and expanding and the FRP jacket is activating, and then a final linear portion that is predominately controlled by the FRP jacket until the ultimate state (i.e. FRP rupture). For the trilinear response, the initial branch continues until an initial peak stress is reached ($\varepsilon'_{c1}, f'_{c1}$), which is marginally greater than the unconfined concrete strength (f'_{co}). Following this is a descending branch where the concrete is laterally expanding at a rapid rate and the concrete core is losing its strength quite rapidly. During this descending portion, the passive confinement provided by the FRP jacket is insufficient in heavily influencing the behaviour of the specimen. Once enough outward expansion of the concrete core has occurred, the FRP jacket eventually provides sufficient confinement to the concrete core and the FRP begins to control the stress-strain response. The transition point between the descending branch and sufficient FRP activation is referred to as

the post-peak ravine stress (ε'_{c2}, f'_{c2}) (Zeng et al. 2020). The final ascending linear branch continues until FRP rupture (ε'_{cu}, f'_{cu}).

The traditional FRP-confined specimens tested in this study exhibited a classical bilinear stress-strain response. In contrast, the majority of LRS FRP-confined HSC and UHSC specimens tested in this study exhibited a trilinear stress-strain response. Similar stress-strain behaviour has been presented in Zeng et al. (2020) for PET FRP-confined concrete. From that study, it is inconclusive whether shrinkage played a role in the strength reduction because prefabricated PET FRP tubes were used. It is anticipated that this trilinear behaviour is caused due to the insufficient confinement pressure provided by the LRS FRP composites at the point of concrete cracking. As the load carrying capacity of the cylinders began to decrease, the confinement pressure required for an ascending branch decreased. As the load-carrying capacity further decreased, the hoop rupture strain in the FRP increased, which in turn increased the confinement pressure. When the confinement pressure had sufficiently increased, the FRP jacket began to effectively confine the concrete core, and the load carrying capacity transitioned from descending to ascending. Additional contribution to the strength reduction could be caused by the delayed confinement action of the FRP due to the minor crimp in the unidirectional fibre due to the existence of weft yarns that hold the fabric together. This crimp was more significant in LRS FRP due to the thickness of the fibre sheet. This was further complicated by the effect of bending which is more pronounced for a thicker jacket.

Key results from this experimental programme are presented in Tables 1-3. The initial peak

stress and strain (f'_{c1} and ε'_{c1}, respectively) and the post-peak ravine stress and strain (f'_{c2} and ε'_{c2}, respectively) were not included for specimens that exhibited a bilinear stress-strain response.

Compressive Behaviour

A means of comparing the behaviour of FRP-confined concrete after the fact is using the actual confinement ratio $f_{l,a}/f'_{co}$, where $f_{l,a} = 2E_f t_f \varepsilon_{h,rup}/D$ is the confinement pressure at the point of FRP rupture. This differs from the nominal confinement ratio (f_l/f'_{co}) as the actual confinement ratio ($f_{l,a}/f'_{co}$) uses the ultimate hoop rupture strain of the FRP jacket obtained from the FRP-confined test specimen ($\varepsilon_{h,rup}$) rather than the FRP rupture strain obtained from coupon tests (ε_f). Due to the bilinear nature of PEN and PET FRP, the actual confinement ratio for LRS FRP-confined concrete is calculated using $f_{l,a}/f'_{co} = 2t_f (E_2\varepsilon_{h,rup} + C_{f,0}) / Df'_{co}$.

The influence the confinement stiffness ratio (ρ_K) has on the stress ratios (i.e. f'_{c1}/f'_{co}, f'_{c2}/f'_{co} and f'_{cu}/f'_{co}) for PEN and PET FRP-confined concrete is shown in Figure 7, where $\rho_K = 2E_f t_f / (f'_{co}/\varepsilon'_{co})D$. It is evident that the initial peak stress (i.e. the point (ε'_{c1}, f'_{c1}) from Figure 6(b)), post-peak ravine stress (i.e. the point (ε'_{c2}, f'_{c2}) from Figure 6(b)), and ultimate stress are all influenced by the confinement stiffness ratio. The confinement stiffness ratio has the biggest influence on the final stress (f'_{cu}) for both the PEN and PET FRP-confined specimens, where increasing the confinement stiffness ratio increases the final stress. Additionally, the post-peak ravine stress is considerably influenced by the confinement stiffness ratio, where the amount of strength reduction reduces (i.e. approaches a value of 1) as the confinement stiffness ratio increases. This shows that by providing additional confining pressure to the concrete core,

strength reduction after initial concrete cracking can be eliminated. The confinement stiffness ratio has the least influence on the initial peak stress, however there is still a positive correlation between the initial peak stress and the confinement stiffness ratio.

It is well understood that the slope of the linear branch after initial concrete cracking is dependent on the confinement stiffness provided by the FRP jacket for traditional FRP-confined specimens with bilinear stress-strain responses (Teng et al. 2009; Yu et al. 2010). This mechanism is understood to be the same for those specimens that exhibit a trilinear response with strength softening, where the slope of the second and third linear branches are dependent on the confinement stiffness. Figure 8 shows the relationship between the gradient of the second and third linear branches and the confinement stiffness ratio (ρ_K). From Figure 8(a-b) it is evident that increasing the confinement stiffness ratio significantly reduces the slope of the second linear branch (i.e. approaches a gradient of 0). This in turn shows that when the confinement stiffness ratio is increased beyond a given threshold, the stress-strain response will become bilinear. It can also be seen for both PEN and PET FRP that the confinement stiffness ratio has a more profound effect on UHSC specimens than HSC specimens, where increasing the confinement stiffness ratio reduces the strength reduction more rapidly. Similarly, Figure 8(c-d) shows that increasing the confinement stiffness ratio will also increase the gradient of the final linear branch. However, the influence that the confinement stiffness ratio has on the final branch is far less pronounced that the effect it has on the descending branch. This can be explained since those specimens with low confinement stiffness ratios will exhibit more significant strength reduction, thus less confinement is needed for an ascending final branch.

Similar to the gradient of the descending branch, the degree of strength reduction after concrete cracking for LRS FRP-confined HSC and UHSC specimens is influenced by the confinement stiffness ratio. Figure 9 shows the relationship between the stress retention ratio (f'_{c2}/f'_{c1}) (i.e. strength reduction after the initial peak stress) and the confinement stiffness ratio (p_K). In this study, for both PEN and PET FRP-confined specimens, increasing the confinement stiffness ratio results in an increase in stress retention. Figure 9 shows as the confinement stiffness ratio approaches a value of 0.03, the stress retention approaches unity (i.e. no strength reduction).

Figure 10 shows the relationship between the strain ratios (i.e. $\varepsilon'_{c1}/\varepsilon'_{co}$, $\varepsilon'_{c2}/\varepsilon'_{co}$ and $\varepsilon'_{cu}/\varepsilon'_{co}$) and the actual confinement ratio ($f_{l,a}/f'_{co}$). It is evident that the ultimate strain is heavily influenced by the actual confinement ratio for both PEN and PET FRP-confined cylinders, where increasing the actual confinement ratio improves the strain capacity of the cylinder. The strain at the initial peak stress (ε'_{c1}) and the post-peak ravine stress (ε'_{c2}) also increase as the actual confinement ratio increases, but at a less significant rate.

Lateral Behaviour

The lateral behaviour of both PEN and PET FRP-confined concrete cylinders are expressed through the hoop strain versus axial strain relationship, as presented in Figure 11. The hoop strain readings presented in these graphs are obtained from the average of the three mid-height lateral strain gauges, whereas the axial strain readings were obtained from the average of the two mid-height LVDT readings. It was found that the hoop strain readings became unreliable at high strain ranges, where a number of strain gauges debonded due to the large deformation

of the FRP. Since the dilation behaviour during the early stages of the test are of most interest, the hoop strain-axial strain relationships are discontinued at the point of strain gauge debonding.

Figure 11(a-c) shows that at initial loading, the hoop strains are very low in comparison to the axial strain readings since the lateral expansion of the concrete core is minimal prior to the point of initial concrete cracking. Following this is a transition point where the FRP begins to engage and the hoop strain increases more rapidly (see TP1 on Figure 11(c)). It is notable across Figure 11(a-c) that as the concrete strength increases, the hoop strain increases at a more rapid rate after this transition point. Afterwards, there is another transition point where there is a diminution in hoop rupture strain increase in comparison to axial strain (see TP2 on Figure 11(c)). This second transition point indicates that the rapid lateral expansion of the concrete core has been stabilised by the FRP jacket. After this second transition point, the hoop strain and axial strain increase at an almost linear rate until failure. This shows that the concrete expands at a more constant rate after this point.

It is shown in Figure 11 that an increase in FRP confinement results in the hoop strain increasing at a slower rate in comparison to the axial strain. This behaviour has been noted by a number of researchers for both traditional FRP- and LRS FRP-confined concrete (Pessiki et al. 2001; Saleem et al. 2017; Zhou et al. 2019; Zeng et al. 2020). This behaviour is less evident as the concrete strength increases and it is anticipated that this is due to the smaller difference in the confinement stiffness ratio between specimens with different numbers of FRP layers. In addition, the lateral expansion of concrete is less uniform as the concrete strength increases due

to localised macrocracks, thus the average hoop strain is less affected.

Figure 12 shows the stress versus axial strain plotted alongside the hoop strain versus axial strain for three PET FRP-confined USHC specimens, using axial strain as a shared horizontal axis. From the magnified section of this graph, the point of initial concrete cracking ($\varepsilon'_{c1}, f'_{c1}$) aligns with the first transition point on the hoop strain-axial strain plot (TP1). Following this transition point is a rapid increase in hoop strain where the load carrying capacity of the specimen is rapidly decreasing. The hoop strain then experiences a second transition point (TP2) where it begins to increase at a slower rate, and this second transition point is shown to align with the post-peak ravine stress ($\varepsilon'_{c2}, f'_{c2}$).

Influence of FRP Type

A means of assessing the effectiveness of an FRP jacket is the strain efficiency factor ($\varepsilon_{h,rup}/\varepsilon_f$). Comprehensive research on the strain efficiency factor of traditional FRP composites has been undertaken, and these values typically fall within 0.60 – 0.90 (Lam and Teng 2003; Smith et al. 2010; Ozbakkaloglu et al. 2013; Wu and Jiang 2013). However, due to the limited number of studies on LRS FRP-confined concrete, these values are not well established for PEN and PET FRP. The strain efficiency factors for PEN and PET FRP-confined concrete tested in this study are plotted in Figure 13(a-b) and are 0.60 and 0.59, respectively. Specimens that failed due to FRP slippage were excluded from these graphs. Strain efficiency factors reported in other studies to date on LRS FRP-confined concrete have varied from 0.50 to 0.95 (Dai et al. 2011; Ispir 2015; Saleem et al. 2017; Zeng et al. 2020). Figure 13(a-b) indicates that those specimens with a low actual confinement ratio (~0.1) have a lower strain efficiency factor than those

specimens that are well-confined, which is consistent with findings from studies on traditional FRP-confined columns (Lim and Ozbakkaloglu 2014). It was noted in this study that the hoop strain distribution of PEN and PET specimens was more non-uniform than the traditional FRP specimens, particularly at higher strain ranges. In addition, due to the thickness of the LRS FRP jacket, tensile and bending stresses are induced in the FRP jacket due to axial load on the FRP jacket. It is anticipated that the combination of these factors resulted in a lower strain efficiency for LRS FRP-confined concrete.

Figures 14-16 compare the influence that different FRP confining materials have on the axial stress-strain behaviour of NSC, HSC and UHSC, respectively. This approach of comparing FRP types using the nominal confinement ratio (f_l/f'_{co}) has been used previously by other researchers (Ozbakkaloglu 2013b; Ozbakkaloglu and Xie 2016). Although it is ideal to compare FRP types with identical nominal confinement ratios, it is often not possible since the only modifiable variable is the number of FRP layers. For this reason, FRP types with nominal confinement ratios as similar as possible are used for comparison. Tables 1-3 show the key test results of the specimens displayed in Figures 14-16.

In Figure 14(a), NSC specimens are confined with one-layer PEN FRP, two-layer GFRP and one-layer AFRP. A similar comparison is shown in Figure 14(b) where NSC confined with two-layers of PEN FRP is compared with two-layer PET FRP. As illustrated in Figure 14(a), the traditional FRP-confined specimens achieve a slightly higher ultimate stress than the LRS FRP-confined counterpart. This can be explained due to a combination of the traditional FRP

composites having a higher strain efficiency factor and higher confining stiffness. However, more significant variation exists in the ultimate strains achieved between the traditional FRP-confined specimens and the LRS FRP-confined specimens, where the latter exhibit much higher ultimate axial strains. Additionally, the second linear branch of the LRS FRP-confined specimens have a gentler gradient than the traditional FRP counterparts because they have a lower confinement stiffness. This shows that specimens with larger rupture strains and equivalent confinement ratios (i.e. LRS FRP specimens) have far more gradual strength increase, and the corresponding stress occurs at a much greater axial strain than the traditional FRP-confined specimens. The same can be seen in Figure 14(b) where the stiffer confining material (i.e. PEN FRP) has a steeper final branch and achieves a lower ultimate strain. This shows the benefit of LRS FRP composites for ductile applications.

In Figure 15(a), HSC specimens are confined with one-layer PEN FRP, one-layer PET FRP and two-layer GFRP. Each specimen exhibits an initial peak stress at concrete cracking, followed by a strength drop. It appears that the GFRP specimen begins to recover from the strength reduction similarly to the LRS FRP specimens, however it fails before significant strength is regained since the strain capacity of the jacket is exceeded. Additionally, it can be seen that stiffer FRP jackets experience less strength reduction after initial concrete cracking. This shows that the trilinear response is not an inherent mechanism of the bilinear LRS FRP, rather a trait of low confinement stiffness and large rupture strain. Similarly in Figure 15(b), the AFRP-confined specimen has an ascending bilinear response, whereas the PEN FRP-confined specimen has a small strength reduction after initial concrete cracking. It is anticipated that the

PEN FRP jacket is on the verge of providing sufficient confinement stiffness to prevent strength reduction, and the fabric structure and thickness of the PEN FRP is causing delayed confinement. This delayed confinement becomes more pronounced when the concrete core becomes stiffer (i.e. the unconfined concrete strength increases). Nonetheless, any minor increases in the confinement stiffness will transition this response from trilinear to bilinear.

The three UHSC specimens shown in Figure 16 were confined with either two-layer PET FRP, two-layer PEN FRP or three-layer CFRP. The CFRP-confined specimen in Figure 16 has an ascending bilinear stress-strain response and ruptures at a low axial strain (~0.01). In contrast, the PET FRP- and PEN FRP-confined specimens experience a trilinear stress-strain response. The degree of strength reduction after concrete cracking is influenced by the confinement stiffness, where the PET FRP specimen experiences greater strength reduction than the PEN FRP specimen. In addition, the third linear branch of both specimens has a similar gradient although the PEN FRP provided a greater confinement stiffness. This is the case since the strength reduction was greater for PET FRP, so the equivalent level of confinement stiffness required to produce a similar slope branch is lower.

Although the confinement mechanism of traditional FRP and LRS FRP composites is similar, the stress-strain behaviour of the specimens confined by these composites is quite different. As such, the use of a given material will vary depending on the application. When enhancing the strength and stiffness is of prime concern, traditional FRP composites appear to be a better alternative. However, when enhancing the strain capacity is of prime concern, such as in seismic

applications, LRS FRP composites appear to be a better alternative.

Influence of Concrete Strength

The nominal confinement ratio (f_l/f'_{co}) is used to directly compare the behaviour of specimens with the same FRP type and different concrete strengths. Since it is difficult to achieve exact nominal confinement ratio comparisons across different concrete strengths, the ratios that are most similar across different concrete strengths are used within reason. Figure 17 compares the influence of concrete strength on the axial behaviour of FRP-confined specimens by showing the normalised axial stress-strain response for FRP-wrapped specimens with different concrete strengths. The normalised axial stress is defined as the stress applied to the FRP-confined specimen (σ_c) divided by the corresponding unconfined concrete strength (f'_{co}).

Figure 17(a-b) shows the effect that concrete strength has on the axial performance of PEN and PET FRP-confined cylinders. The results show that when the nominal confinement ratio (f_l/f'_{co}) is similar across different concrete strengths, the unconfined concrete strength affects the strength enhancement ratio (f'_{cu}/f'_{co}). As the unconfined concrete strength increases, the strength enhancement ratio and ultimate strain decrease. In addition, the relative stress at initial concrete cracking is influenced by the unconfined concrete strength, particularly for the NSC specimens. This can be explained since the confinement stiffness ratio is higher for the NSC specimens at the point of concrete cracking, and lower strength concrete requires less confinement for the same level of strength enhancement. Similar findings are shown in Figure 17(c-d) for traditional FRP-confined concrete. These findings are consistent with those from other researchers that have compared the influence of concrete strength on the performance of

traditional FRP-confined concrete (Ozbakkaloglu 2013b; Lim and Ozbakkaloglu 2015).

The compressive response of PEN FRP-confined concrete provided in Figure 17(a) transitions from an ascending bilinear response for the NSC specimen to a trilinear response with strength reduction once the unconfined concrete strength increases to high strength. Similarly in Figure 17(b) for two-layer PET FRP-confined HSC and four-layer PET FRP-confined UHSC, increasing the unconfined concrete strength results in additional strength reduction. This shows that as the unconfined concrete strength increases, the amount of relative confinement provided by the FRP jacket must increase to achieve the same performance in terms of strength retention. However, the unconfined concrete strength appears to have little influence on the slope of the final linear branch for PET FRP specimens in Figure 17(b). This is anticipated since the UHSC specimen experienced additional strength reduction, thus the relative level of confinement required for an ascending branch is lower.

Influence of Additional FRP Layers

Figures 18 to 20 show the influence that the number of FRP layers has on the axial stress-strain response of NSC, HSC and UHSC confined with different FRP jackets. Key test parameters and results for the specimens are shown in Tables 1 to 3.

Figure 18(a) shows that for CFRP-confined NSC specimens, as the number of FRP layers increase, the ultimate stress and strain capacity of the cylinder increases. Figure 18(b-c) shows that PEN and PET FRP-confined cylinders behave in a similar manner, where the ultimate stress and axial strain increase as the number of FRP layers increase. Similar observations are noted

in Figures 19 and 20 for HSC and UHSC concrete, respectively. It is also evident for NSC confined concrete of all FRP types that the slope of the second linear branch becomes steeper when additional FRP layers are added. This shows that when concrete is sufficiently confined, the traditional FRP- and LRS FRP-confined specimens respond similarly to increasing amounts of confinement stiffness (i.e. increases in FRP layers).

As illustrated in Figure 19(a-c), the traditional FRP-confined HSC cylinders exhibit increasing ultimate stress and axial strain when additional FRP layers are added. The influence of confinement is also visually evident in the second linear branch of the stress-strain response of these specimens, where several specimens transitioned from a descending branch to an ascending branch as the number of FRP layers are increased. Additionally, regardless of the FRP type, the initial peak stress on the stress-strain response occurs at a higher axial stress as additional FRP layers are added. However, behaviour of the LRS FRP-confined cylinders after this initial peak stress are somewhat different to the traditional FRP-confined specimens. After initial concrete cracking, the LRS-confined samples exhibit a strength reduction before the FRP provides sufficient confinement. The magnitude of the strength reduction experienced after the initial peak stress decreases as the number of FRP layers increase (i.e. confinement stiffness is increased). Similar behaviour is experienced in Figure 20 for LRS FRP-confined UHSC specimens. This indicates that by increasing the number of FRP layers (i.e. confinement stiffness), the strength reduction after initial concrete cracking can be eliminated. This is consistent with that shown in Figure 9.

An observation for LRS FRP-confined HSC and UHSC is that the number of FRP layers has a significant effect on the slope of the descending branch, however there is lesser influence on the slope of the final linear branch of the stress-strain response. With FRP-confined specimens that exhibit a bilinear response, the slope of the final linear branch is directly related to the confinement stiffness provided by the FRP jacket (Figure 18). However, for those specimens that experience a trilinear response, increasing the confinement stiffness (i.e. increasing FRP layers) has little influence on the slope of the final linear branch (Figure 19(d-e) and Figure 20). This behaviour can be attributed to the fact that specimens with a lower amount of FRP confinement experience greater strength reductions after initial concrete cracking, resulting in lesser confinement needed at the same equivalent strain level.

Conclusions

The results of 66 FRP-confined concrete specimens tested under monotonic axial compression have been presented herein. The variables investigated in this study were fibre type, fibre thickness and concrete strength. The test programme consisted of both traditional FRP- and LRS FRP-confined concrete cylinders, and the unconfined concrete strengths ranged from NSC to HSC to UHSC. Based on the results obtained from experimentation, the following conclusions are drawn:

1. The generalised stress-strain behaviour of LRS FRP-confined NSC is monotonically ascending and bilinear in nature. Once the concrete strength is high, however, the stress-strain response becomes trilinear with a strength reduction after initial concrete cracking. The severity of strength reduction is dependent on the confinement provided by the FRP

jacket.

2. Attributed to their large rupture strains and low elastic modulus, PEN and PET FRP can significantly improve the ductility of concrete with a relatively lesser increase in compressive strength in comparison to traditional FRPs. A significant relationship exists between the ultimate axial strain of the fibres and the ultimate axial strain of the FRP-confined cylinders constructed using them.
3. HSC and UHSC specimens sufficiently confined with LRS FRP can exhibit high deformation capacities. The level of confinement necessary to effectively confine concrete increases as the unconfined concrete strength increases.
4. The lateral dilation behaviour of LRS FRP-confined concrete consists of two almost-linear portions, connected by a transition zone. The start and end of the transition zone align with the initial peak stress and the post-peak ravine stress, respectively. The steepness of this transition zone is influenced by the unconfined concrete strength, where higher strength concrete causes a more rapid lateral expansion of concrete. Increasing the confinement stiffness ratio (i.e. FRP layers) reduces the slope of this transition zone.
5. Traditional FRP composites are more efficient than LRS FRP composites in terms of the FRP strain efficiency factor. Increasing the actual confinement ratio resulted in an increase in the strain efficiency factor.
6. The confinement of concrete with LRS FRP composites is effective in regard to the ultimate strength and ultimate strain enhancements. The LRS FRP-confined specimens had strength enhancements of slightly lower value than the comparable traditional FRP-confined specimen with a similar confinement ratio. Additionally, the ultimate strain enhancement

of the LRS FRP-confined specimens was far higher than that of the comparable traditional FRP-confined specimens.

7. In general, adding additional LRS FRP layers improves the strength and ultimate axial strain of the cylinder. Furthermore, for those specimens that exhibited a trilinear stress-strain response, the amount of strength reduction after concrete cracking reduced when additional FRP layers were provided.

The present study has been limited to short columns without any internal reinforcement. Experimental tests on full-scale specimens confined with LRS FRP composites should be conducted in the future to understand the effect of scalability. Significantly thick FRP jackets will be required for full-scale specimens and hence testing is essential to understand behaviour at this scale. The inclusion of internal reinforcement should also be considered to understand the influence that restraining longitudinal bars has on the confinement mechanism of LRS FRP.

Data Availability Statement

All data, models, and code that support the findings of this study are available from the corresponding author upon reasonable request.

Acknowledgements

The authors gratefully acknowledge the financial support provided by the Australian Research Council via a Discovery grant (DP170102992). The authors also thank Messrs Zi Sheng Tang and Connor Johnston for their valuable contribution to the experimental testing.

Notation

The following symbols are used in this paper:

$C_{f,0}$ = constant strength value where the extrapolation of the second linear branch intersects the stress axis;

D = diameter of concrete core;

E_f = elastic modulus of FRP jacket;

E_1 = first elastic modulus of bilinear FRP jacket;

E_2 = second elastic modulus of bilinear FRP jacket;

f'_{c1} = initial peak stress;

f'_{c2} = post-peak ravine stress;

f'_{c2}/f'_{c1} = stress retention ratio;

f'_{cm} = maximum axial stress;

f'_{co} = unconfined concrete strength;

f'_{cu} = ultimate axial stress;

f'_{cm}/f'_{co} = strength enhancement ratio;

f_f = ultimate tensile stress of FRP;

f_l = ultimate confining pressure (based on ε_f);

f_l/f'_{co} = nominal confinement ratio;

$f_{l,a}$ = actual confining pressure (based on $\varepsilon_{h,rup}$);

$f_{l,a}/f'_{co}$ = actual confinement ratio;

t_f = total nominal thickness of FRP jacket;

ε'_{c1} = axial strain at initial peak stress;

ε'_{c2} = axial strain at post-peak ravine stress;

ε'_{co} = axial strain at unconfined concrete strength;

ε'_{cu} = ultimate axial strain;

$\varepsilon_{h,rup}$ = hoop rupture strain in FRP jacket at specimen failure;

$\varepsilon_{h,rup}/\varepsilon_f$ = strain efficiency factor;

ε_f = tensile strain capacity of FRP obtained from coupon tests;

$\varepsilon_{f,0}$ = strain value where two linear branches of bilinear response intersect;

ρ_K = confinement stiffness ratio;

σ_c = stress applied to FRP-confined specimen; and

σ_f = stress applied to FRP tension coupon.

References

Anggawidjaja, D., T. Ueda, J. Dai, and H. Nakai. 2006. "Deformation capacity of RC piers wrapped by new fiber-reinforced polymer with large fracture strain." *Cement and Concrete Composites*. 28 (10): 914-927. https://doi.org/10.1016/j.cemconcomp.2006.07.011

AS (Standards Australia). 2014. *Compressive Strength Tests – Concrete, Mortar and Grout Specimens.* AS1012.9. Sydney, AU: Standards Australia.

AS (Standards Australia). 2014. *Preparing Concrete Mixes in the Laboratory*. AS1012.2. Sydney, AU: Standards Australia.

ASTM (American Society of Testing and Materials). 2017. *Standard Test Method for Determining Tensile Properties of Fiber Reinforced Polymer Matrix Composites Used for Strengthening of Civil Structures*. ASTM D 7565. West Conshohocken, PA: ASTM.

Bai, Y. L., J. G. Dai, and J. G. Teng. 2014. "Cyclic compressive behavior of concrete confined with large rupture strain FRP composites." *Journal of Composites for Construction*. 18 (1): 04013025. https://doi.org/10.1061/(ASCE)CC.1943-5614.0000386

Bai, Y. L., J. G. Dai, M. Mohammadi, G. Lin, and S. J. Mei. 2019. "Stiffness-based design-oriented compressive stress-strain model for large-rupture-strain (LRS) FRP-confined concrete." *Composite Structures*. 223 (Sep): 110953. https://doi.org/10.1016/j.compstruct.2019.110953

Dai, J. G., Y. L. Bai, and J. G. Teng. 2011. "Behavior and modeling of concrete confined with FRP composites of large deformability." *Journal of Composites for Construction*. 15 (6): 963-973. https://doi.org/10.1061/(ASCE)CC.1943-5614.0000230

Han, Q., W. Yuan, Y. Bai, and X. Du. 2020. "Compressive behavior of large rupture strain (LRS)

FRP-confined square concrete columns: experimental study and model evaluation." *Materials and Structures.* 53 (99): 1-20. https://doi.org/10.1617/s11527-020-01534-4

Isleem, H. F., Z. Wang, D. Wang, and S. T. Smith. 2018. "Monotonic and cyclic axial compressive behavior of CFRP-confined rectangular RC columns." *Journal of Composites for Construction*. 22 (4): 04018023. https://doi.org/10.1061/(ASCE)CC.1943-5614.0000860

Ispir, M. 2015. "Monotonic and cyclic compression tests on concrete confined with PET-FRP." *Journal of Composites for Construction*. 19 (1): 04014034. https://doi.org/10.1061/(ASCE)CC.1943-5614.0000490

Ispir, M., K. D. Dalgic, and A. Ilki. 2018. "Hybrid confinement of concrete through use of low and high rupture strain FRP." *Composites Part B: Engineering.* 153 (Nov): 243-255. https://doi.org/10.1016/j.compositesb.2018.07.026

Jiang, T., and J. G. Teng. 2007. "Analysis-oriented stress–strain models for FRP–confined concrete." *Engineering Structures*. 29 (11): 2968-2986. https://doi.org/10.1016/j.engstruct.2007.01.010

Lam, L., and J. G. Teng. 2003. "Design-oriented stress–strain model for FRP-confined concrete." *Construction and Building Materials*. 17 (6-7): 471-489. https://doi.org/10.1016/S0950-0618(03)00045-X

Lim, J. C., and T. Ozbakkaloglu. 2014. "Hoop strains in FRP-confined concrete columns: experimental observations." *Materials and Structures*. 48 (9): 2839-2854. https://doi.org/10.1617/s11527-014-0358-8

Lim, J. C., and T. Ozbakkaloglu. 2015. "Influence of concrete age on stress– strain behavior of

FRP-confined normal- and high-strength concrete." *Construction and Building Materials*. 82 (May): 61-70. https://doi.org/10.1016/j.conbuildmat.2015.02.020

Ozbakkaloglu, T. 2013a. "Behavior of square and rectangular ultra high-strength concrete-filled FRP tubes under axial compression." *Composites Part B: Engineering.* 54 (Nov): 97-111. http://doi.org/10.1016/j.compositesb.2013.05.007

Ozbakkaloglu, T. 2013b. "Compressive behavior of concrete-filled FRP tube columns: Assessment of critical column parameters." *Engineering Structures*. 51 (Jun), 188-199. http://doi.org/10.1016/j.engstruct.2013.01.017

Ozbakkaloglu, T., and E. Akin. 2012. "Behavior of FRP-confined normal- and high-strength concrete under cyclic axial compression." *Journal of Composites for Construction*. 16 (4): 451-463. https://doi.org/10.1061/(ASCE)CC.1943-5614.0000273

Ozbakkaloglu, T., and T. Xie. 2016. "Geopolymer concrete-filled FRP tubes: Behavior of circular and square columns under axial compression." *Composites Part B: Engineering.* 96 (Jul): 215-230. http://dx.doi.org/10.1016/j.compositesb.2016.04.013

Ozbakkaloglu, T., J. C. Lim., and T. Vincent. 2013. "FRP-confined concrete in circular sections: Reivew and assessment of stress-strain models." *Engineering Structures*. 49 (Apr): 1068-1088. http://dx.doi.org/10.1016/j.engstruct.2012.06.010

Pessiki, S., K. A. Harries, J. T. Kestner, R. Sause, and J. M. Ricles. 2001. "Axial behavior of reinforced concrete columns confined with FRP jackets." *Journal of Composites for Construction*. 5 (Nov): 237-245. https://doi.org/10.1061/(ASCE)1090-0268(2001)5:4(237)

Saleem, S., Q. Hussain, and A. Pimanmas. 2017. "Compressive behavior of PET FRP–confined circular, square, and rectangular concrete columns." *Journal of Composites for*

Construction. 21 (3): 04016097. https://doi.org/10.1061/(ASCE)CC.1943-5614.0000754

Saleem, S., A. Pimanmas, and W. Rattanapitikon. 2018. "Lateral response of PET FRP-confined concrete." *Construction and Building Materials*. 159 (Jan): 390-407. https://doi.org/10.1016/j.conbuildmat.2017.10.116

Smith, S. T., S. J. Kim, and H. Zhang. 2010. "Behavior and effectiveness of FRP wrap in the confinement of large concrete cylinders." *Journal of Composites for Construction*. 15 (5), 573-582. https://doi.org/10.1061/(ASCE)CC.1943-5614.0000119

Teng, J. G., J. F. Chen, S. T. Smith, and L. Lam. 2002. *FRP-Strengthened RC Structures*. West Sussex, UK: John Wiley & Sons.

Teng, J. G., T. Jiang, L. Lam, and Y. Z. Luo. 2009. "Refinement of a design-oriented stress-strain model for FRP-confined concrete." *Journal of Composites for Construction*. 13 (4): 269-278. https://doi.org/10.1061/(ASCE)CC.1943-5614.0000012

Vincent, T., and T. Ozbakkaloglu. 2013. "Influence of concrete strength and confinement method on axial compressive behavior of FRP confined high- and ultra high-strength concrete." *Composites Part B: Engineering*. 50 (Jul): 413-428. http://doi.org/10.1016/j.compositesb.2013.02.017

Wang, W., C. Wu, and Z. Liu. 2019. "Compressive behavior of hybrid double-skin tubular columns with ultra-high performance fiber-reinforced concrete (UHPFRC)." *Engineering Structures*. 180 (Feb): 419-441. https://doi.org/10.1016/j.engstruct.2018.11.048

Wu, Y. F., and J. F. Jiang. 2013. "Effective strain of FRP for confined circular concrete columns." *Composite Structures*. 95 (Feb): 479-491. http://doi.org/10.1016/j.compstruct.2012.08.021

Xiao, Q. G., J. G. Teng, and T. Yu. 2010. "Behavior and modeling of confined high-strength concrete." *Journal of Composites for Construction*. 14 (3): 249-259. https://doi.org/10.1061/(ASCE)CC.1943-5614.0000070

Xiao, Y., and H. Wu. 2003. "Compressive behavior of concrete confined by various types of FRP composite jackets." *Journal of Reinforced Plastic and Composites*. 22 (13): 1187-1201. https://doi.org/10.1177/0731684403035430

Xie, T., and T. Ozbakkaloglu. 2015. "Behavior of steel fiber-reinforced high-strength concrete-filled FRP tube columns under axial compression." *Engineering Structures*. 90 (May): 158-171. http://doi.org/10.1016/j.engstruct.2015.02.020

Yu, T., J. G. Teng, Y. L. Wong, and S. L. Dong. 2010. "Finite element modeling of confined concrete-I: Drucker–Prager type plasticity model." *Engineering Structures*. 32 (3): 665-679. https://doi.org/10.1016/j.engstruct.2009.11.014

Zeng, J. J., G. Lin, J. G. Teng, and L. J. Li. 2018. "Behavior of large-scale FRP-confined rectangular RC columns under axial compression." *Engineering Structures*. 174 (Nov): 629-645. https://doi.org/10.1016/j.engstruct.2018.07.086

Zeng, J. J., Y. Y. Ye, W. Y. Gao, S. T. Smith, and Y. C. Guo. 2020. "Stress-strain behavior of polyethylene terephthalate fiber-reinforced polymer-confined normal-, high- and ultra high-strength concrete." *Journal of Building Engineering*. 30 (Jul): 101243. https://doi.org/10.1016/j.jobe.2020.101243

Zhang, B., X. M. Hu, Q. Zhao, T. Huang, N. Y. Zhang, and Q. B. Zhang. 2020. "Effect of fiber angles on normal- and high-strength concrete-filled fiber-reinforced polymer tubes under monotonic axial compression." *Advances in Structural Engineering*. 23 (5): 924-940.

https://doi.org/10.1177/1369433219886082

Zhang, D., Y. Zhao, W. Jin, T. Ueda, and H. Nakai. 2017a. "Shear strengthening of corroded reinforced concrete columns using pet fiber based composties." *Engineering Structures*. 153 (Dec): 757-765. https://doi.org/10.1016/j.engstruct.2017.09.030

Zhang, B., J. G. Teng, and T. Yu. 2017b. "Compressive behavior of double-skin tubular columns with high-strength concrete and a filament-wound FRP tube." *Journal of Composites for Construction*. 21 (5): 04017029. https://doi.org/10.1061/(ASCE)CC.1943-5614.0000800

Zhou, Y., Y. Zheng, L. Sui, F. Xing, J. Hu, and P. Li. 2019. "Behavior and modeling of FRP-confined ultra-lightweight cement composites under monotonic axial compression." *Composites Part B: Engineering*. 162 (Apr): 289-302. https://doi.org/10.1016/j.compositesb.2018.10.087

Table 1: Experimental results for FRP-confined normal-strength concrete specimens

Specimen ID [#]	Fibre Type	Layers	f'_{co} (MPa)	ε'_{co}	f_l/f'_{co}	f'_{cu} (MPa)	ε'_{cu} (%)	f'_{cm}/f'_{co}	$\varepsilon'_{cu}/\varepsilon'_{co}$	$\varepsilon_{h,rup}/\varepsilon_f$
A-NS-1-a	Aramid	1	20.9	0.0019	0.42	54.1	2.15	2.59	11.32	0.77
A-NS-1-b [1]	Aramid	1	20.9	0.0019	0.42	39.9	1.05	1.91	5.53	0.31
C-NS-1-a	Carbon	1	20.9	0.0019	0.24	42.3	1.28	2.02	6.74	0.79
C-NS-1-b	Carbon	1	20.9	0.0019	0.24	43.4	1.40	2.08	7.37	0.97
C-NS-2-a	Carbon	2	20.9	0.0019	0.49	63.5	2.06	3.04	10.84	0.98
C-NS-2-b	Carbon	2	20.9	0.0019	0.49	59.0	1.82	2.82	9.58	0.87
G-NS-1-a	Glass	1	20.9	0.0019	0.20	30.9	1.55	1.51	8.16	0.90
G-NS-1-b	Glass	1	20.9	0.0019	0.20	32.1	1.39	1.54	7.32	0.82
G-NS-2-a	Glass	2	20.9	0.0019	0.41	49.8	2.38	2.38	12.53	0.98
G-NS-2-b	Glass	2	20.9	0.0019	0.41	48.5	2.27	2.32	11.95	0.79
PEN-NS-1-a[1]	PEN	1	20.9	0.0019	0.41	31.8	1.26	1.59	6.63	0.20
PEN-NS-1-b	PEN	1	20.9	0.0019	0.41	45.3	5.21	2.21	27.42	0.75
PEN-NS-2-a	PEN	2	20.9	0.0019	0.81	65.5	5.71	3.13	30.05	0.63
PEN-NS-2-b[2]	PEN	2	20.9	0.0019	0.81	59.5	5.76	2.85	30.32	0.41
PET-NS-2-a	PET	2	20.9	0.0019	0.75	53.1	6.71	2.55	35.32	0.60
PET-NS-2-b[2]	PET	2	20.9	0.0019	0.75	60.8	8.24	2.91	43.37	0.58
PET-NS-3-a[1, 2]	PET	3	20.9	0.0019	1.12	65.2	6.22	3.12	32.74	0.39
PET-NS-3-b[2]	PET	3	20.9	0.0019	1.12	68.1	7.70	3.26	40.53	0.54

[#] Specimen ID: FRP type (A = aramid, C = carbon, G = glass, PEN = polyethylene naphthalate, PET = polyethylene terephthalate) - Concrete strength (NS = normal strength, HS = high strength, UHS = ultra-high strength) - Number of FRP layers (e.g. 1 = 1 layer, 2 = 2 layers) - Nominally identical specimens (a or b).

[1]Failure caused by FRP slippage; [2]Hoop strain gauges failed prematurely

Table 2: Experimental results for FRP-confined high-strength concrete specimens

Specimen ID	Fibre Type	Layers	f'_{co} (MPa)	ε'_{co}	f_l/f'_{co}	f'_{cu} (MPa)	ε'_{cu} (%)	f'_{c1} (MPa)	ε'_{c1} (%)	f'_{c2} (MPa)	ε'_{c2} (%)	f'_{cm}/f'_{co}	$\varepsilon'_{cu}/\varepsilon'_{co}$	$\varepsilon_{h,rup}/\varepsilon_f$
A-HS-1-a [1]	Aramid	1	52.7	0.0021	0.16	55.4	0.82	-	-	-	-	1.18	3.90	0.26
A-HS-1-b	Aramid	1	52.7	0.0021	0.16	59.6	1.00	-	-	-	-	1.19	4.76	0.64
A-HS-2-a	Aramid	2	52.7	0.0021	0.33	90.1	2.08	-	-	-	-	1.71	9.90	0.72
A-HS-2-b	Aramid	2	52.7	0.0021	0.33	79.3	1.65	-	-	-	-	1.50	7.86	0.78
C-HS-1-a	Carbon	1	52.7	0.0021	0.10	46.8	0.76	-	-	-	-	1.16	3.62	0.78
C-HS-1-b	Carbon	1	52.7	0.0021	0.10	52.9	0.69	-	-	-	-	1.23	3.29	0.82
C-HS-2-a	Carbon	2	52.7	0.0021	0.19	79.4	1.08	-	-	-	-	1.51	5.14	0.94
C-HS-2-b	Carbon	2	52.7	0.0021	0.19	78.1	1.11	-	-	-	-	1.48	5.29	0.81
G-HS-1-a	Glass	1	52.7	0.0021	0.08	35.2	1.22	-	-	-	-	0.94	5.81	0.73
G-HS-1-b	Glass	1	52.7	0.0021	0.08	35.1	1.22	-	-	-	-	1.10	5.81	0.90
G-HS-2-a	Glass	2	52.7	0.0021	0.16	54.2	1.27	-	-	-	-	1.10	6.05	0.76
G-HS-2-b	Glass	2	52.7	0.0021	0.16	53.2	1.49	-	-	-	-	1.07	7.10	0.94
G-HS-3-a	Glass	3	52.7	0.0021	0.24	67.0	1.52	-	-	-	-	1.28	7.24	0.74
G-HS-3-b	Glass	3	52.7	0.0021	0.24	74.7	2.07	-	-	-	-	1.42	9.86	0.80
PEN-HS-1-a	PEN	1	52.7	0.0021	0.16	47.7	3.59	54.4	0.48	44.0	1.38	1.03	17.10	0.56
PEN-HS-1-b[1]	PEN	1	52.7	0.0021	0.16	37.8	3.56	60.2	0.37	42.3	0.81	1.14	16.95	0.57
PEN-HS-2-a	PEN	2	52.7	0.0021	0.32	61.2	5.33	66.0	0.60	64.7	1.03	1.48	25.38	0.69
PEN-HS-2-b	PEN	2	52.7	0.0021	0.32	76.4	3.94	67.3	1.02	65.8	1.69	1.46	18.76	0.66
PEN-HS-3-a	PEN	3	52.7	0.0021	0.48	102.6	5.61	74.1	1.00	72.2	1.45	1.95	26.71	0.61
PEN-HS-3-b[1,2]	PEN	3	52.7	0.0021	0.48	95.3	3.67	-	-	-	-	1.81	17.48	0.36
PET-HS-1-a	PET	1	52.7	0.0021	0.15	30.7	3.64	50.1	0.59	38.9	0.84	0.93	17.33	0.50
PET-HS-1-b[1]	PET	1	52.7	0.0021	0.15	32.4	3.99	56.1	0.47	28.2	1.27	1.06	19.00	0.45

PET-HS-2-a	PET	2	52.7	0.0021	0.30	82.3	7.93	62.7	0.46	52.0	1.91	1.56	37.76	0.83
PET-HS-2-b	PET	2	52.7	0.0021	0.30	62.0	7.70	58.1	0.54	47.3	1.53	1.18	36.67	0.91
PET-HS-3-a[2]	PET	3	52.7	0.0021	0.44	81.2	6.19	65.3	0.69	60.6	1.55	1.54	29.48	0.36
PET-HS-3-b	PET	3	52.7	0.0021	0.44	76.5	6.66	62.1	1.38	60.0	1.61	1.45	31.71	0.54

[1]Failure caused by FRP slippage; [2]Hoop strain gauges failed prematurely

Table 3: Experimental results for FRP-confined ultra-high-strength concrete specimens

Specimen ID	FRP Type	Layers	f'_{co} (MPa)	ε'_{co}	f_l/f'_{co}	f'_{cu} (MPa)	ε'_{cu} (%)	f'_{c1} (MPa)	ε'_{c1} (%)	f'_{c2} (MPa)	ε'_{c2} (%)	f'_{cm}/f'_{co}	$\varepsilon'_{cu}/\varepsilon'_{co}$	$\varepsilon_{h,rup}/\varepsilon_f$
A-UHS-1-a	Aramid	1	110.6	0.0026	0.08	86.8	1.07	-	-	-	-	0.95	4.12	0.43
A-UHS-1-b	Aramid	1	110.6	0.0026	0.08	99.4	1.21	-	-	-	-	0.98	4.65	0.59
C-UHS-2-a	Carbon	2	110.6	0.0026	0.09	108.6	0.97	-	-	-	-	1.24	3.73	0.75
C-UHS-2-b	Carbon	2	110.6	0.0026	0.09	120.0	1.07	-	-	-	-	1.10	4.12	0.54
C-UHS-3-a	Carbon	3	110.6	0.0026	0.14	124.6	1.31	-	-	-	-	1.21	5.04	0.78
C-UHS-3-b	Carbon	3	110.6	0.0026	0.14	120.3	1.01	-	-	-	-	1.08	3.89	0.67
G-UHS-2-a	Glass	2	110.6	0.0026	0.08	82.0	1.15	-	-	-	-	1.12	4.42	0.72
G-UHS-2-b	Glass	2	110.6	0.0026	0.08	65.8	1.44	-	-	-	-	1.02	5.54	0.69
G-UHS-3-a	Glass	3	110.6	0.0026	0.12	78.6	1.49	-	-	-	-	0.96	5.73	0.78
G-UHS-3-b	Glass	3	110.6	0.0026	0.12	110.0	0.69	-	-	-	-	0.99	2.65	0.30
PEN-UHS-1-a	PEN	1	110.6	0.0026	0.08	55.6	3.35	101.1	0.69	51.0	1.69	0.91	12.88	0.53
PEN-UHS-1-b	PEN	1	110.6	0.0026	0.08	56.6	3.75	106.6	0.37	45.5	1.18	0.96	14.42	0.60
PEN-UHS-2-a	PEN	2	110.6	0.0026	0.15	93.7	3.95	113.1	0.81	90.6	1.06	1.02	15.19	0.52
PEN-UHS-2-b	PEN	2	110.6	0.0026	0.15	99.0	2.65	119.3	0.49	84.6	1.10	1.08	10.19	0.62
PEN-UHS-3-a[1]	PEN	3	110.6	0.0026	0.23	122.7	4.40	122.2	0.82	112.6	1.08	1.11	16.92	0.39
PEN-UHS-3-b	PEN	3	110.6	0.0026	0.23	122.9	3.66	130.0	0.48	100.9	1.10	1.18	14.08	0.56
PET-UHS-2-a	PET	2	110.6	0.0026	0.14	98.2	6.56	114.9	0.52	69.2	1.23	1.04	25.23	0.64
PET-UHS-2-b	PET	2	110.6	0.0026	0.14	96.5	6.37	118.2	0.51	63.9	1.20	1.07	24.50	0.64
PET-UHS-3-a	PET	3	110.6	0.0026	0.21	126.9	7.28	134.7	0.46	83.9	1.62	1.22	28.00	0.66
PET-UHS-3-b[1]	PET	3	110.6	0.0026	0.21	96.0	7.00	113.9	0.89	84.9	2.10	1.03	26.92	0.33
PET-UHS-4-a	PET	4	110.6	0.0026	0.28	140.8	6.89	125.7	0.66	96.3	1.67	1.28	26.50	0.57
PET-UHS-4-b	PET	4	110.6	0.0026	0.28	133.3	7.90	122.2	0.82	94.2	1.96	1.30	30.38	0.63

[1]Hoop strain gauges failed prematurely

Table 4: Tensile test results from FRP and epoxy coupons

Material	Nominal thickness (mm/ply)	First stage elastic modulus (E_1) (GPa)	Second stage elastic modulus (E_2) (GPa)	Ultimate strain (ε_f)	Tensile strength (f_f) (MPa)	Constant strength value ($C_{f,0}$) (MPa)	Strain at transition ($\varepsilon_{f,0}$)
Aramid FRP	0.288	107.6	-	0.021	2010	-	-
Carbon FRP	0.13	227.0	-	0.013	3059	-	-
Glass FRP	0.17	85.9	-	0.022	1752	-	-
PEN FRP	0.848	28.3	11.2	0.062	750	120	0.0086
PET FRP	0.841	18.9	7.2	0.086	696	80	0.0075
Epoxy	-	3.6	-	0.029	74.6	-	-

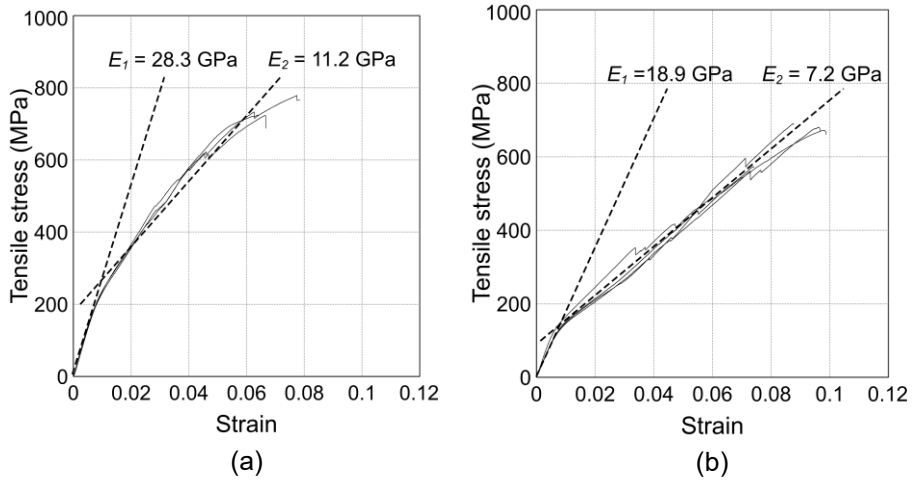

Figure 1: Stress-strain responses of tensile coupons: (a) PEN FRP; (b) PET FRP

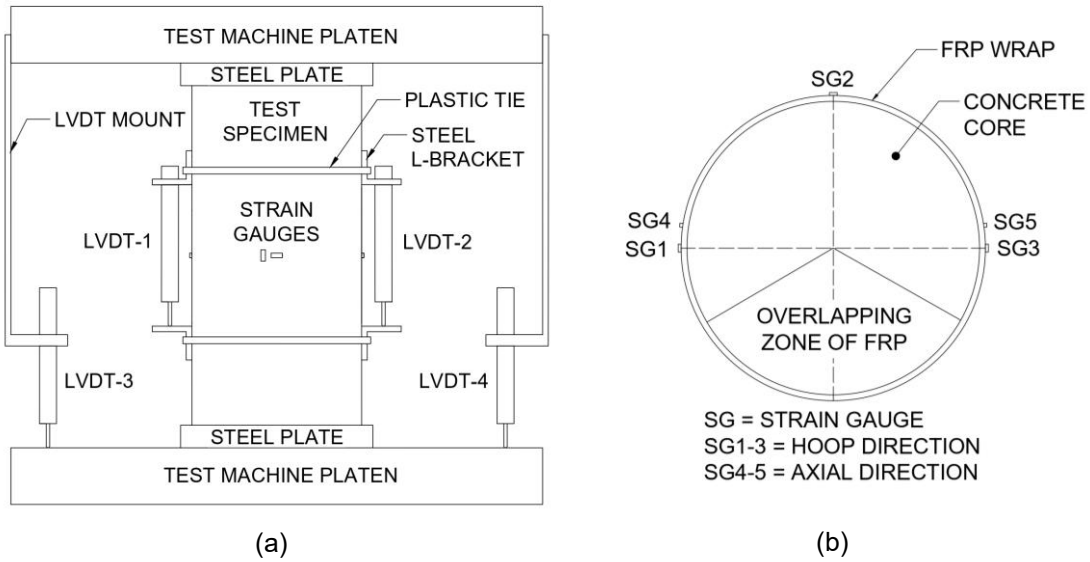

Figure 2: Test instrumentation layout: (a) LVDTs; (b) strain gauges (mid-height)

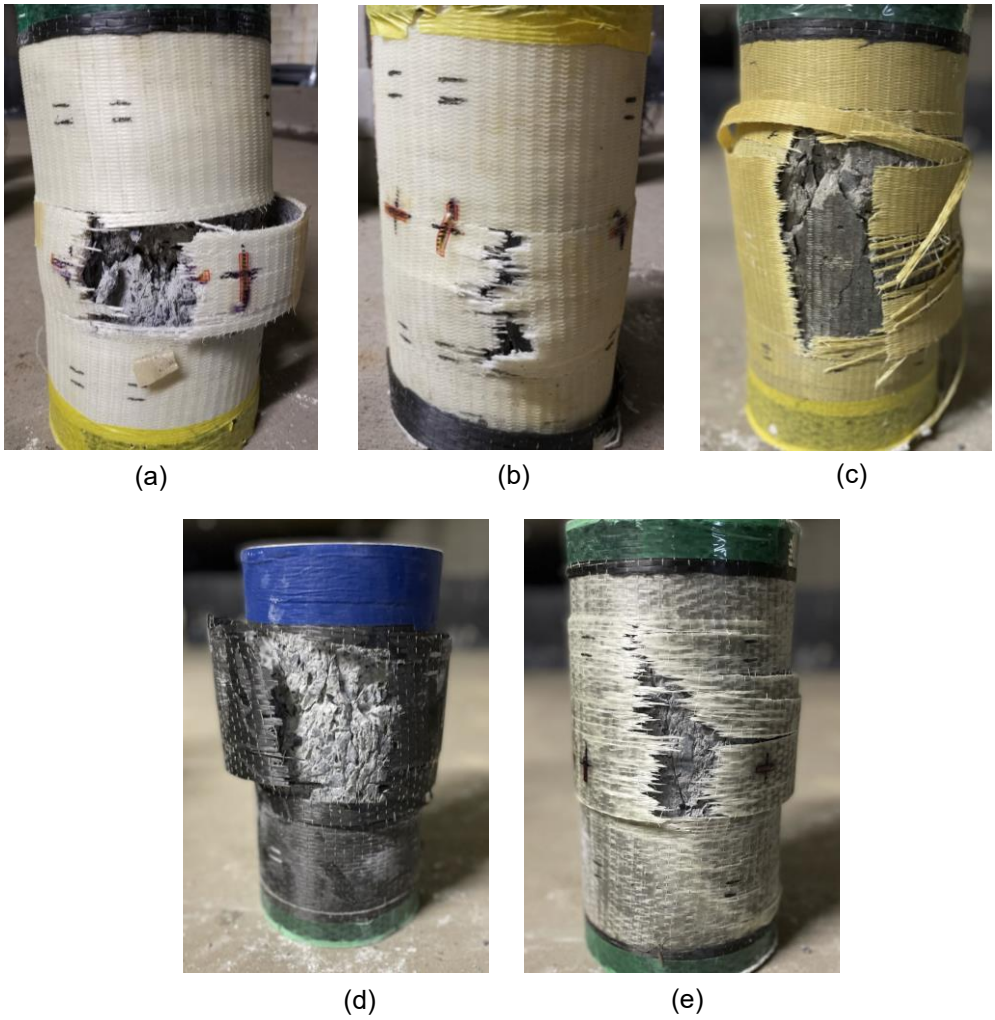

Figure 3: Typical failure modes of FRP-confined specimens: (a) PEN FRP-confined HSC; (b) PET FRP-confined HSC; (c) AFRP-confined UHSC; (d) CFRP-confined HSC; (e) GFRP-confined NSC

(a) (b) (c)

Figure 4: Typical internal failure modes across different concrete strengths: (a) GFRP-confined NSC; (b) CFRP-confined HSC; (c) GFRP-confined UHSC

(a) (b)

Figure 5: Typical FRP slippage failures for LRS FRP-confined concrete: (a) PEN FRP-confined NSC; (b) PET FRP-confined HSC

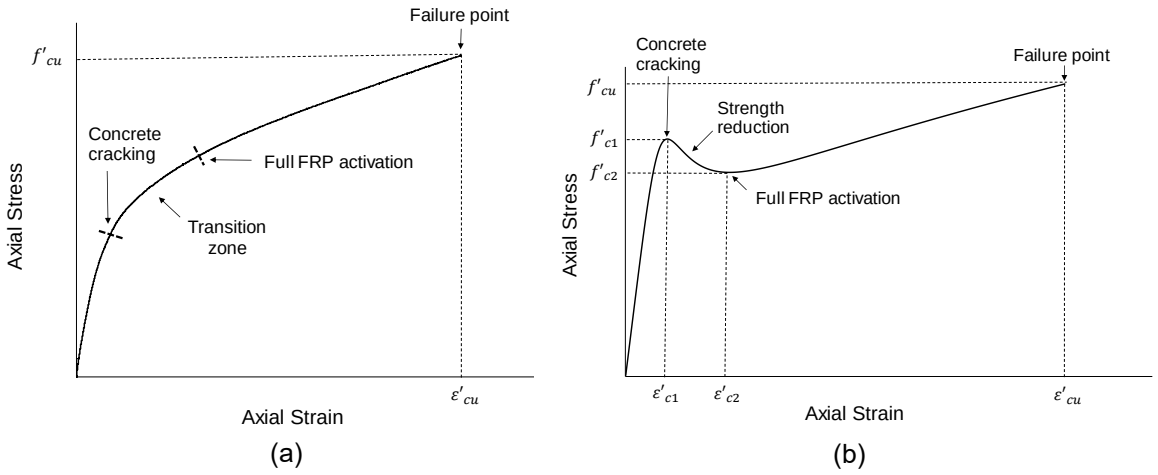

Figure 6: Idealised axial stress-strain responses: (a) traditional FRP-confined concrete; (b) LRS FRP-confined concrete

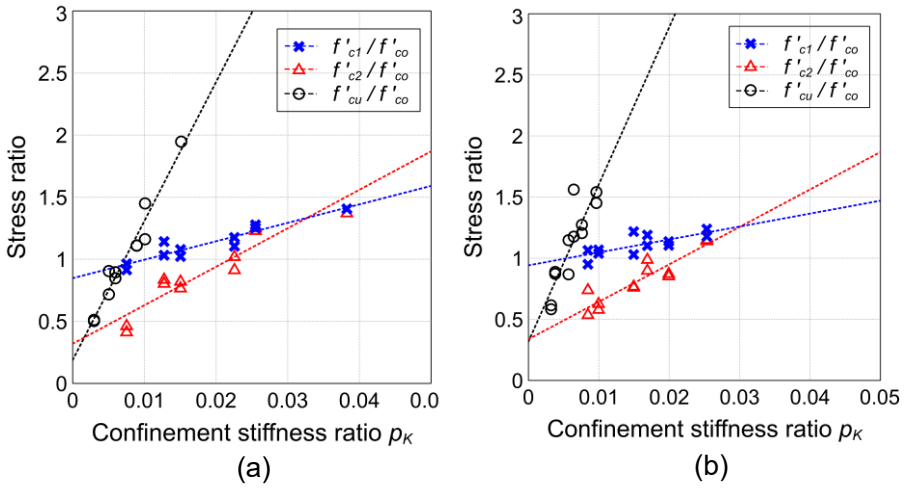

Figure 7: Relationship between stress ratio (i.e. f_{c1}/f'_{co}, f'_{c2}/f'_{co} and f'_{cu}/f'_{co}) and confinement stiffness ratio: (a) PEN FRP-confined concrete; (b) PET FRP-confined concrete

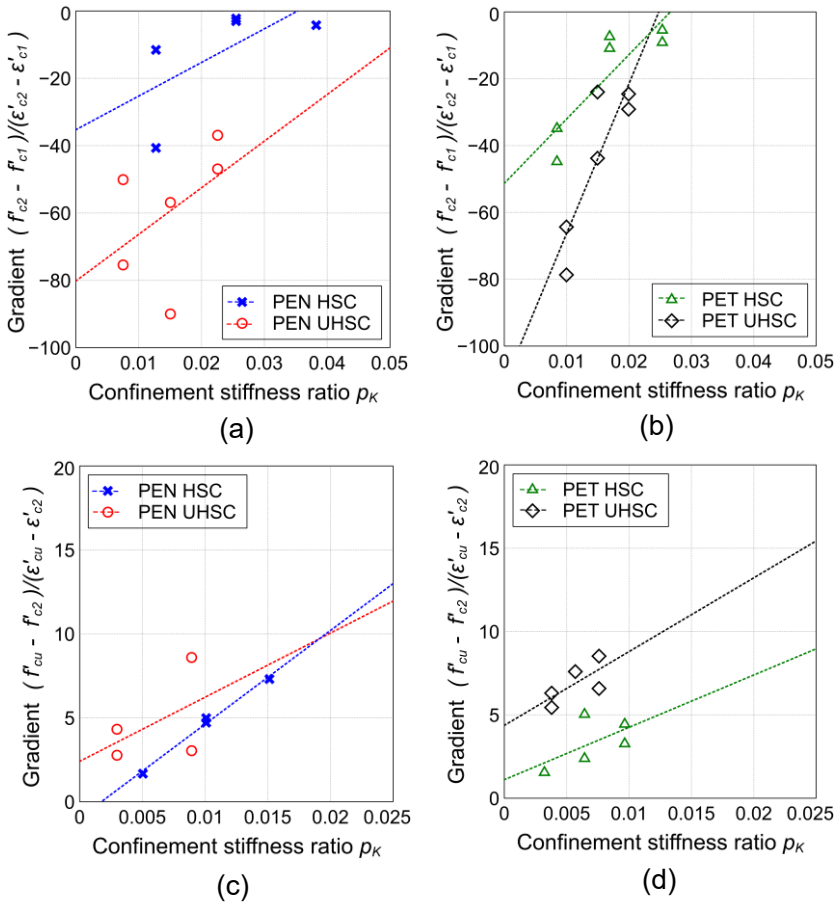

Figure 8: Relationship between gradient of linear branch and the confinement stiffness ratio: (a) PEN FRP second linear branch (i.e. strength reduction); (b) PET FRP second linear branch; (c) PEN FRP third linear branch; (d) PET FRP third linear branch

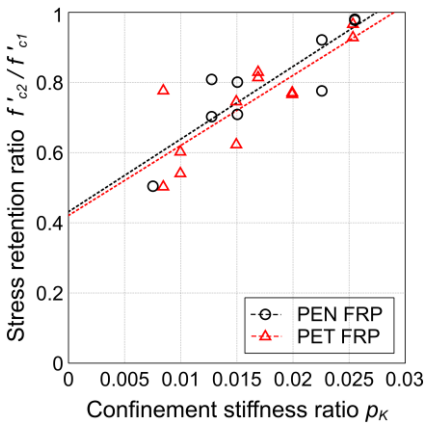

Figure 9: Relationship between stress retention ratio and confinement stiffness ratio for PEN FRP-confined concrete and PET FRP-confined concrete

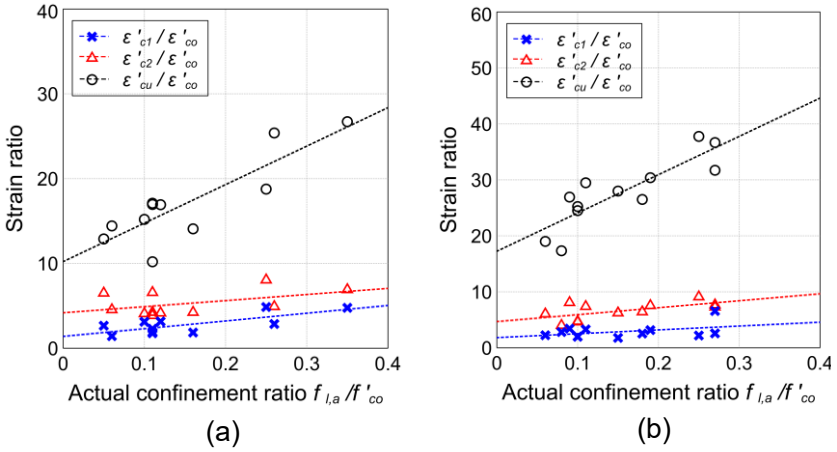

Figure 10: Relationship between strain ratio (i.e. $\varepsilon_{c1}/\varepsilon'_{co}$, $\varepsilon'_{c2}/\varepsilon'_{co}$ and $\varepsilon'_{cu}/\varepsilon'_{co}$) and actual confinement ratio: (a) PEN FRP-confined concrete; (b) PET FRP-confined concrete

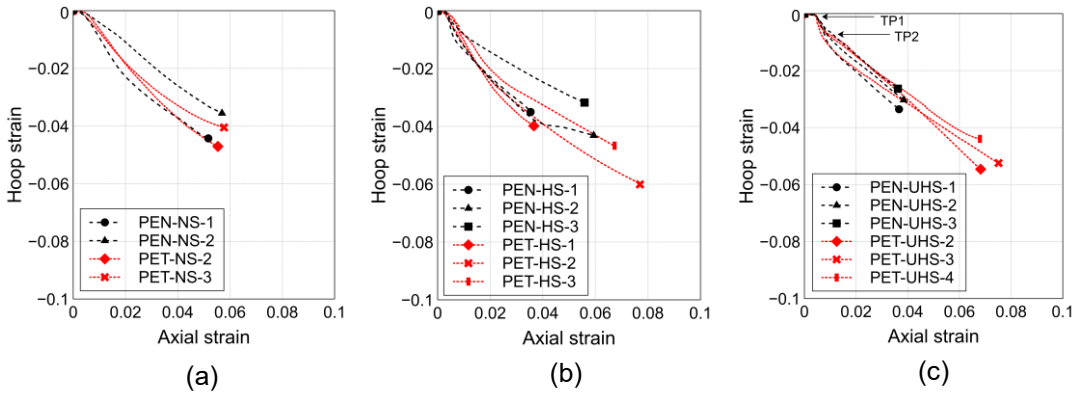

Figure 11: Axial strain-hoop strain relationship of LRS FRP-confined concrete specimens:

(a) NSC; (b) HSC; (c) UHSC

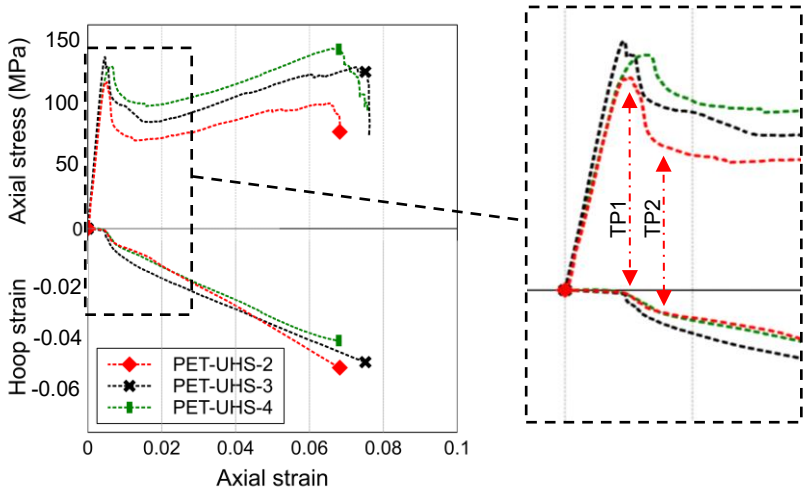

Figure 12: Axial strain-hoop strain behaviour of PET FRP-confined UHSC

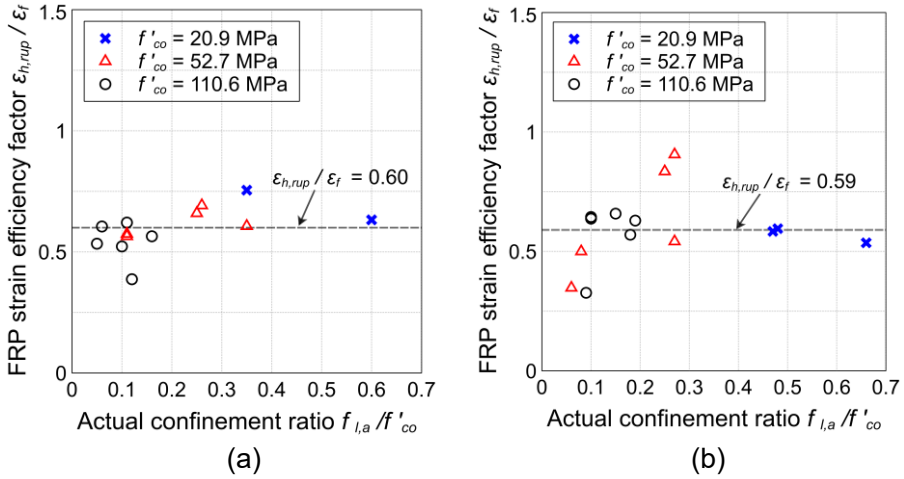

Figure 13: Relationship between FRP strain efficiency factor and actual confinement ratio:

(a) PEN FRP-confined concrete; (b) PET FRP-confined concrete

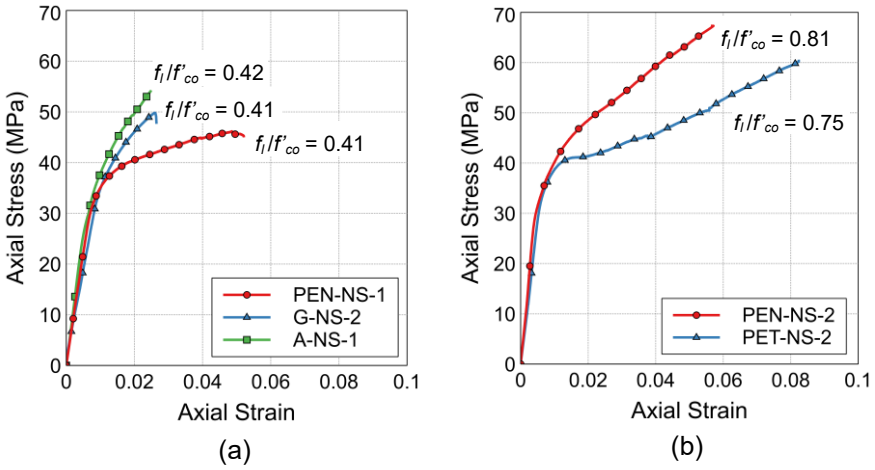

Figure 14: Influence of FRP type on axial stress-strain response of FRP-confined NSC:

(a) Comparison 1: PEN FRP, GFRP and AFRP; (b) Comparison 2: PEN FRP and PET FRP

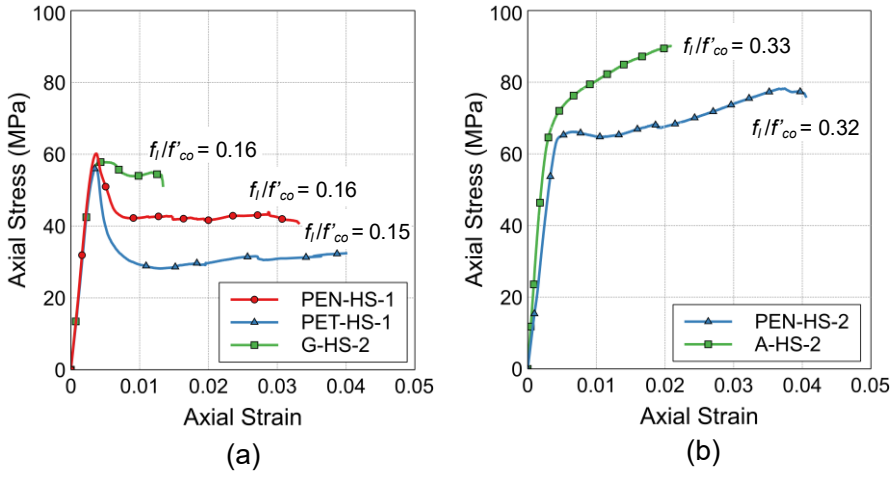

Figure 15: Influence of FRP type on axial stress-strain behaviour of FRP-confined HSC:

(a) Comparison 1: PEN FRP, PET FRP and GFRP; (b) Comparison 2: PEN FRP and AFRP

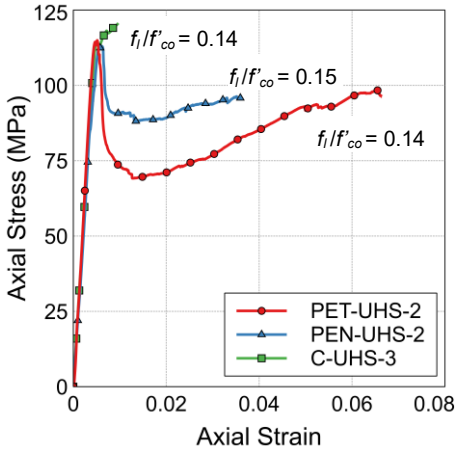

Figure 16: Influence of FRP type on axial stress-strain performance of FRP-confined UHSC.

Comparison: PET FRP, PEN FRP and CFRP

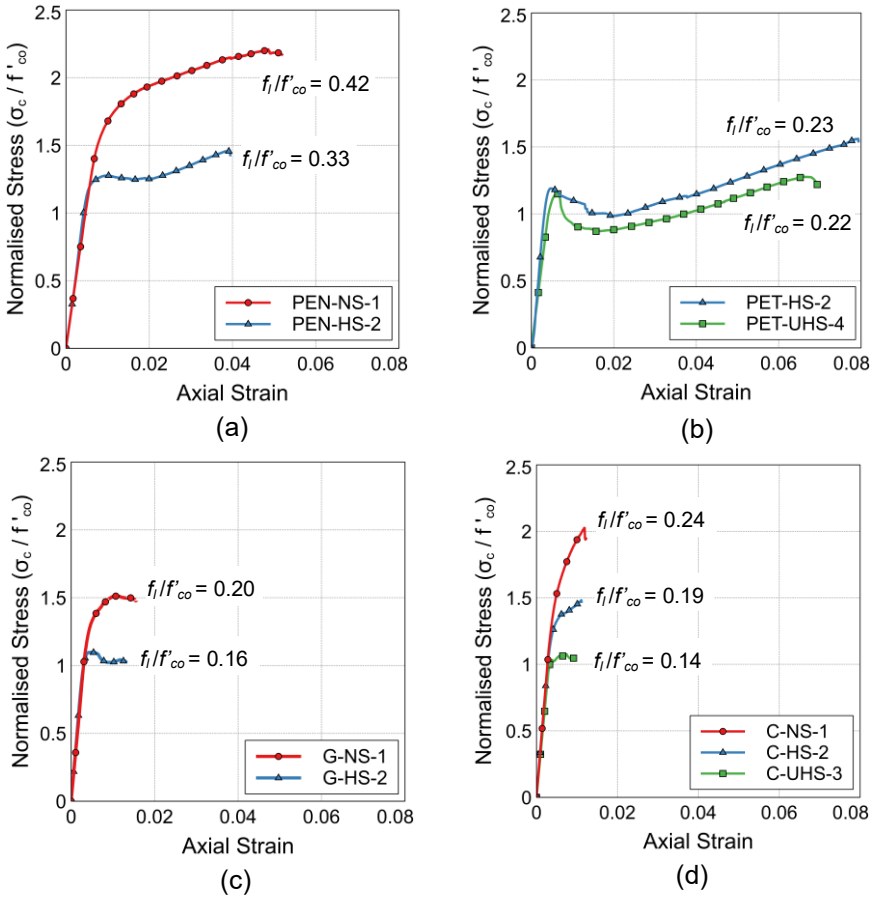

Figure 17: Effect of concrete strength on axial stress-strain performance of FRP-confined specimens: (a) PEN FRP; (b) PET FRP; (c) GFRP; (d) CFRP

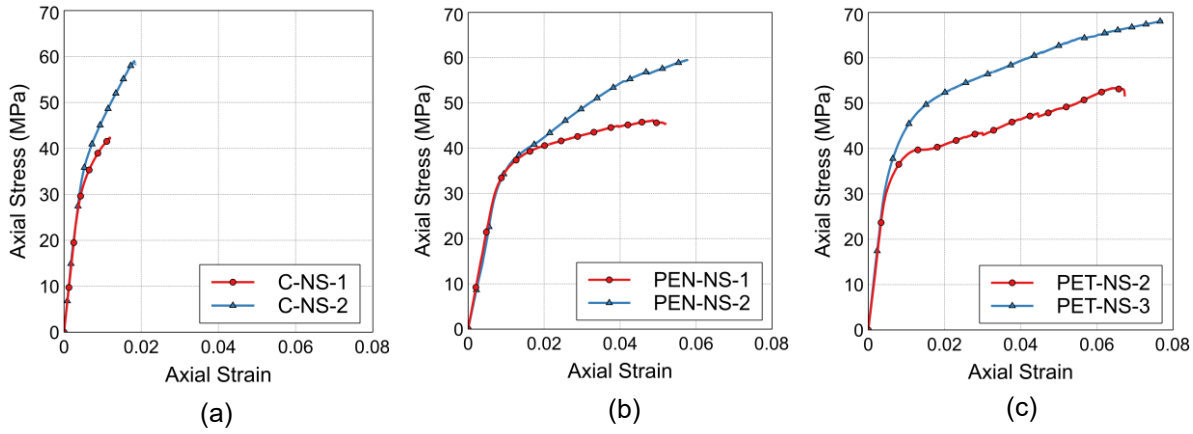

Figure 18: Influence of number of FRP layers on axial performance of FRP-confined NSC:

(a) CFRP; (b) PEN FRP; (c) PET FRP

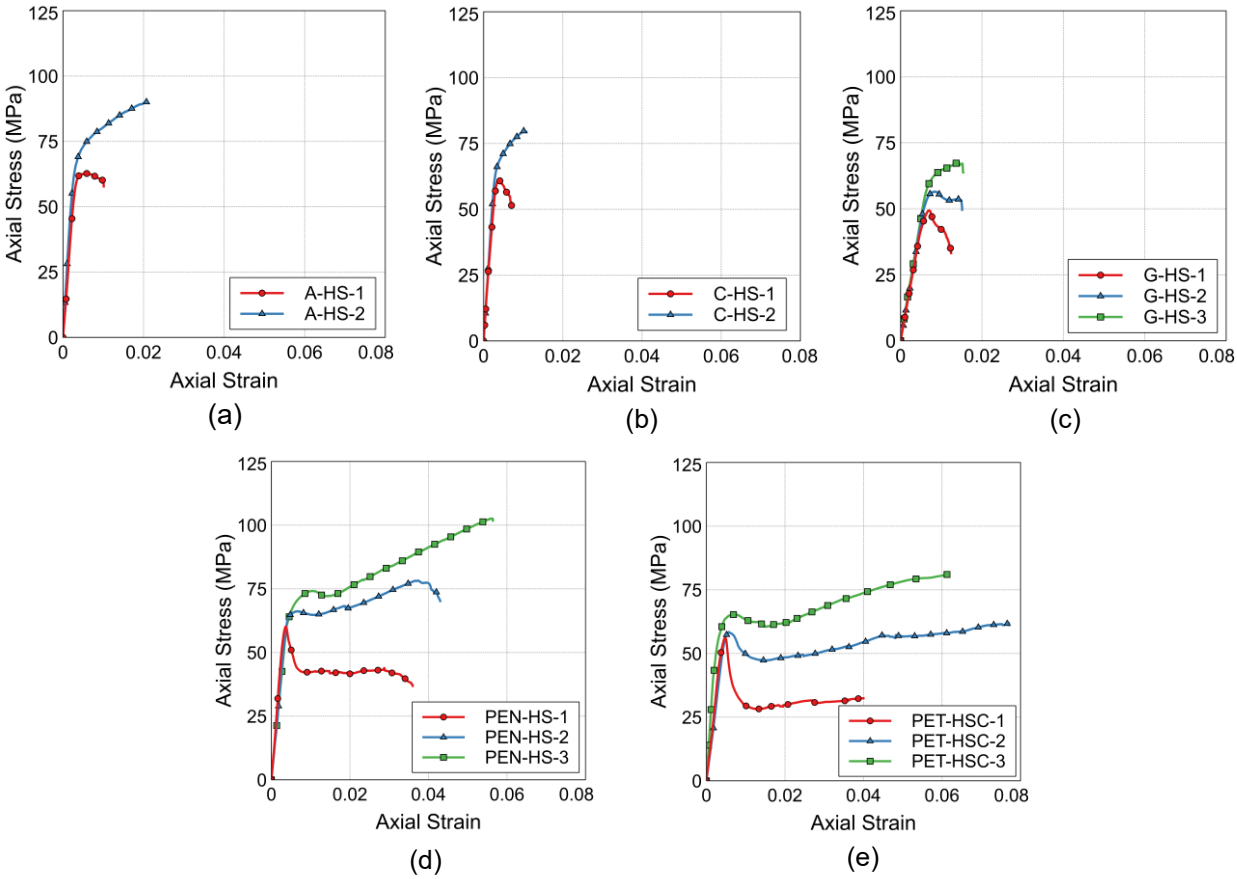

Figure 19: Influence of number of FRP layers on axial performance of FRP-confined HSC:

(a) AFRP; (b) CFRP; (c) GFRP; (d) PEN FRP; (e) PET FRP

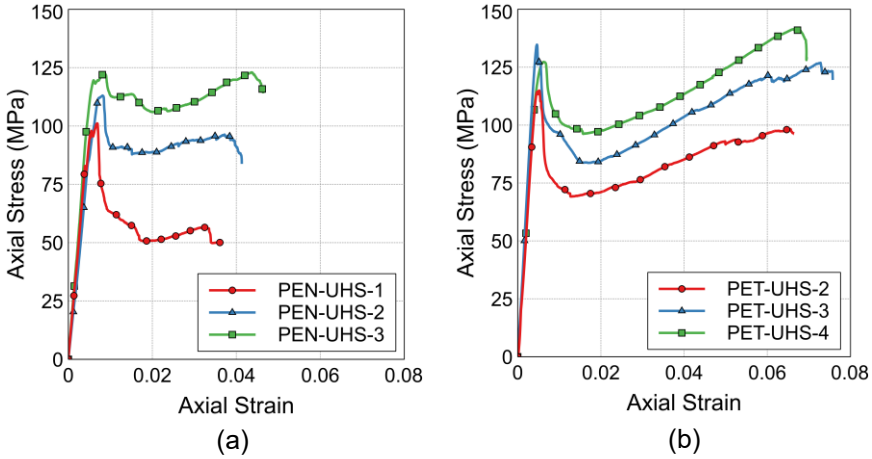

Figure 20: Influence of number of FRP layers on axial performance of LRS FRP-confined UHSC: (a) PEN FRP; (b) PET FRP